Supporting Information

for

High electrical conductivity in directionally polymerized C_{60} nanowires by grazing incidence single particle

Masaki Nobuoka[1,2], S. Sakaguchi[1], Minori Kawata[1], Akie Taguchi[1], Kosuke Kishida[1], Yusuke Tsutsui[1,3], Masayuki Suda[1,4], Haruka Inoue[1], Akira Idesaki[2], Tetsuya Yamaki[2], and Shu Seki[1,5*]

[1]Department of Molecular Engineering, Kyoto University, Kyoto University Katsura, Nishikyo-ku, Kyoto 615-8510, Japan

[2]Takasaki Institute for Advanced Quantum Science, National Institutes for Quantum Science and Technology, Watanuki-machi, Takasaki, Gumma 370-1292, Japan

[3]JST-PRESTO, Honcho 4-1-8, Kawaguchi, Saitama 332-0012, Japan

[4]JST-FOREST, Honcho 4-1-8, Kawaguchi, Saitama 332-0012, Japan

[5]JST-CREST, Honcho 4-1-8, Kawaguchi, Saitama 332-0012, Japan

1. Supplementary Note

This section will discuss vertical devices in detail. For the vertical device, Ti (2 nm) and Au (50 nm) were deposited on a Si substrate by sputtering, and then the organic molecules were deposited by vacuum evaporation. After that, the ion beam irradiation was applied under the same conditions as the main text. In addition, Au was deposited as the top electrode with a diameter of 5 mm. This is because when the nanowires were isolated, they entered the gaps between the nanowires during the deposition of the upper electrode, causing a electrical conduction problem. The organic molecular membrane itself is almost completely insulating, and it is clear that it selectively conducts to the nanowires within the film (Fig. S5). The vertical device that was created was measured with two terminals. The equipment and conditions used are basically the same as in the main text.

2.1. Poor horizontal orientation of soft nanowires

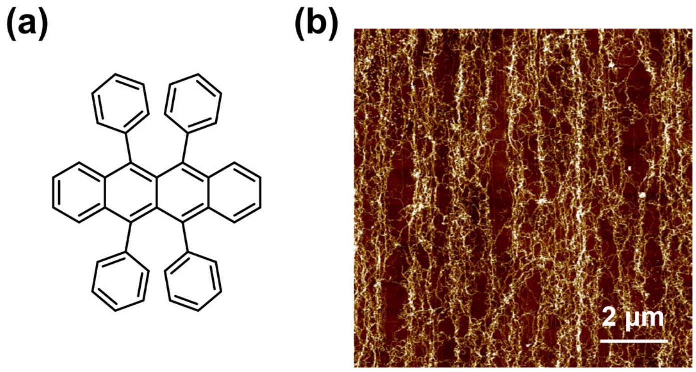

Fig. S1. Fabrication of horizontally-aligned nanowire arrays by high-energy charged particle irradiation. (a) Molecular structure of rubrene. (b) AFM image of horizontally-aligned rubrene-based nanowire arrays at the fluence of 1×10^{11} cm^{-2}. The thickness of irradiated rubrene films was 500 nm.

2.2. Calculation of the radius of C_{60} nanowires

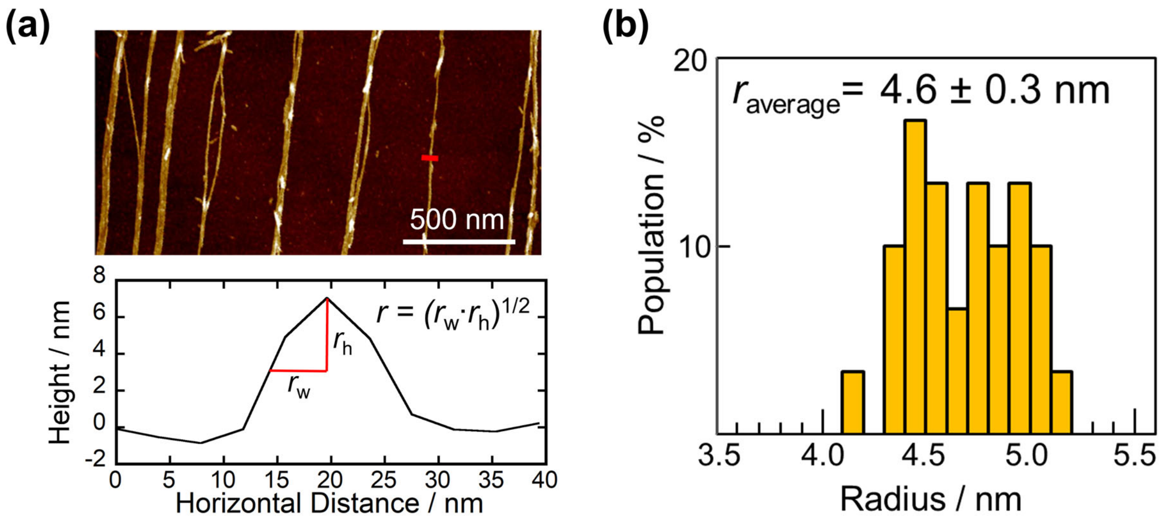

Fig. S2. Fabrication of horizontally-aligned nanowire arrays by high-energy charged particle irradiation. (a) Molecular structure of rubrene. (b) AFM image of horizontally-aligned rubrene-based nanowire arrays at the fluence of 1×10^{11} cm^{-2}. The thickness of irradiated rubrene films was 500 nm.

2.3. Monte Carlo simulation of ion beams

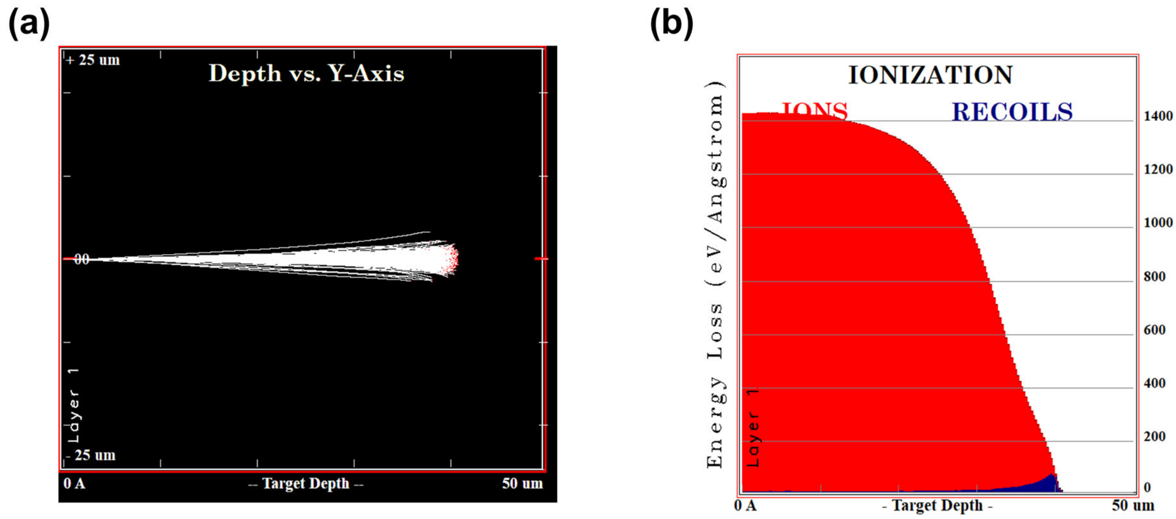

Fig. S3. Monte Carlo simulations of 450 MeV $^{129}Xe^{23+}$ beams in C_{60} thin films. (a) Ion trajectory and (b) LET vs, target depth profile, of 450 MeV $^{129}Xe^{23+}$ beams for 50 µm film thickness of C_{60}. The density of C_{60} was set to 1.72 g/cm^3 by its single crystal.

2.4. Parallel circuits in horizontal devices with nanowire conduction paths

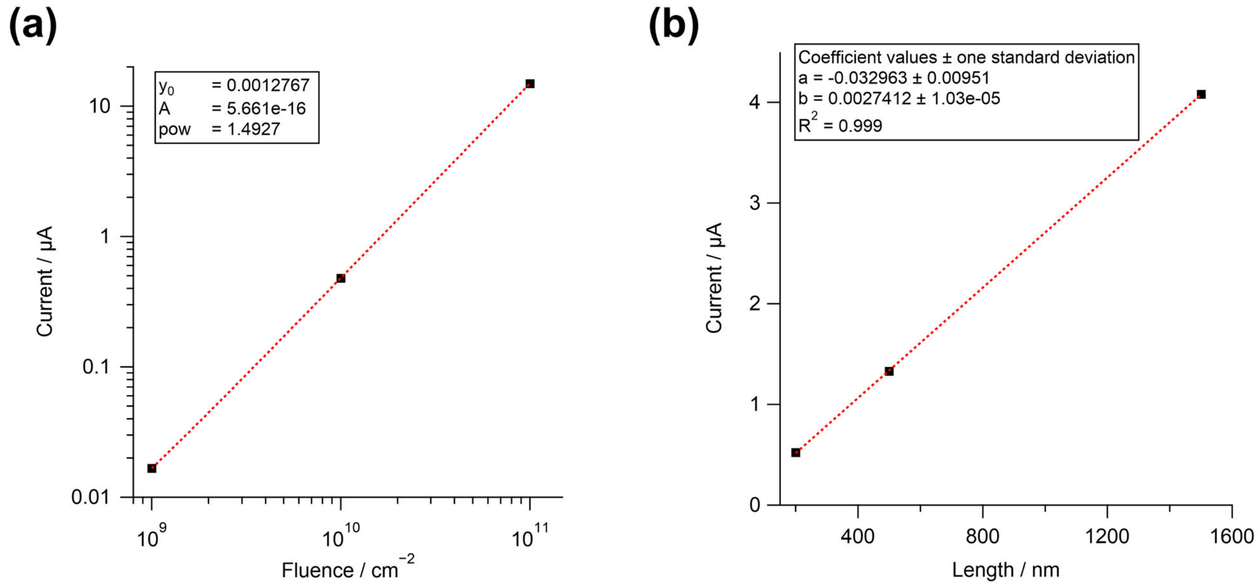

Fig. S4. Increase in current relative to the number of nanowires. Plots of current at +1 V for (a) Fig. 2(b) and (b) Fig. 2(c), respectively. The red dotted lines are all approximated by straight lines.

2.5. Parallel circuits in vertical devices with nanowire conduction paths

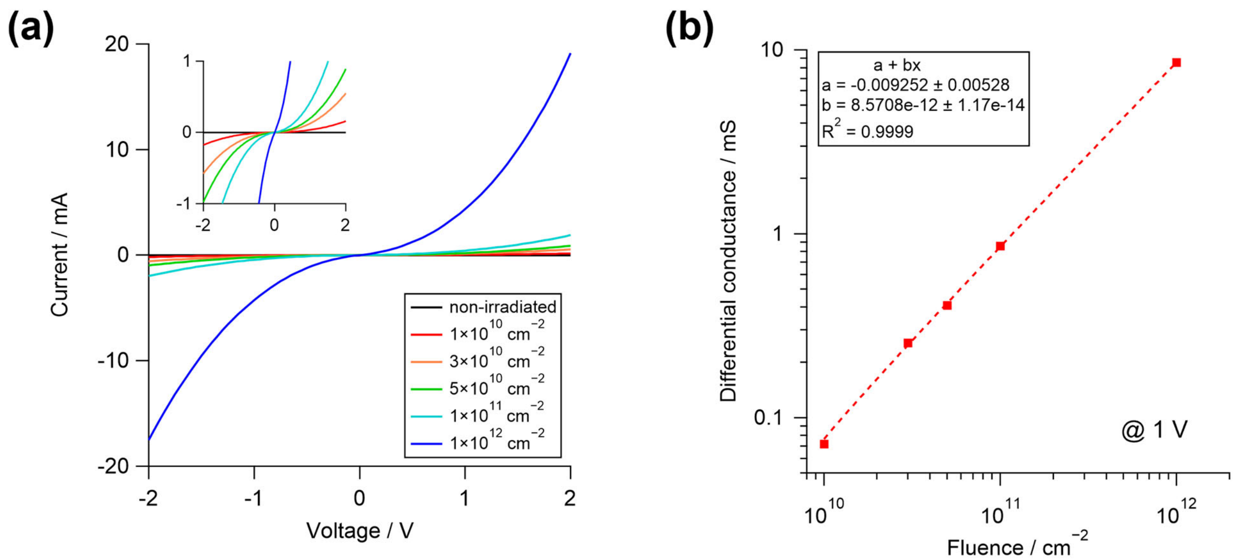

Fig. S5. Current-voltage (*I-V*) characteristics of C_{60} nanowire vertical devices. (a) *I-V* curves for non-irradiated and/or various irradiation fluences. The inset shows an enlarged image. (b) Differential conductance at the applied voltage +1 V, relative to the fluence.

2.6. **Rectification properties of p/n heterojunction nanowires**

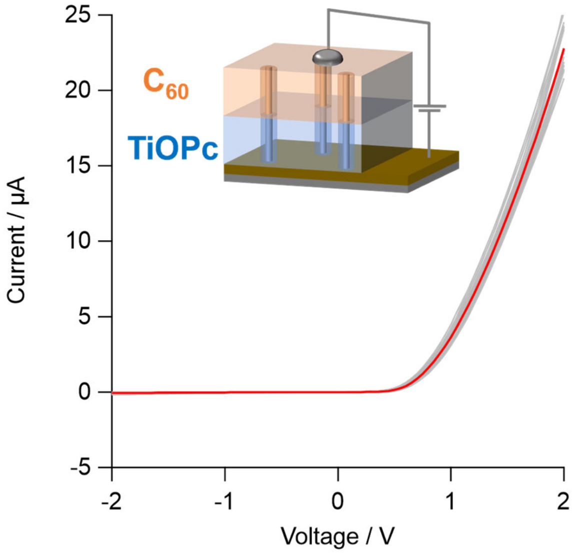

Fig. S6. Current-voltage (*I-V*) characteristics of TiOPc-C_{60} hetero-nanowire vertical devices. Schematic illustration and *I-V* curves of this system at the fluence of 5×10^{10} cm^{-2}. The data shows 20 measurements (gray) and their average (red). In this bilayer, 600 nm thickness of TiOPc and C_{60} were deposited sequentially.

2.7. Calculation of electrical resistivity of a single C_{60} nanowire

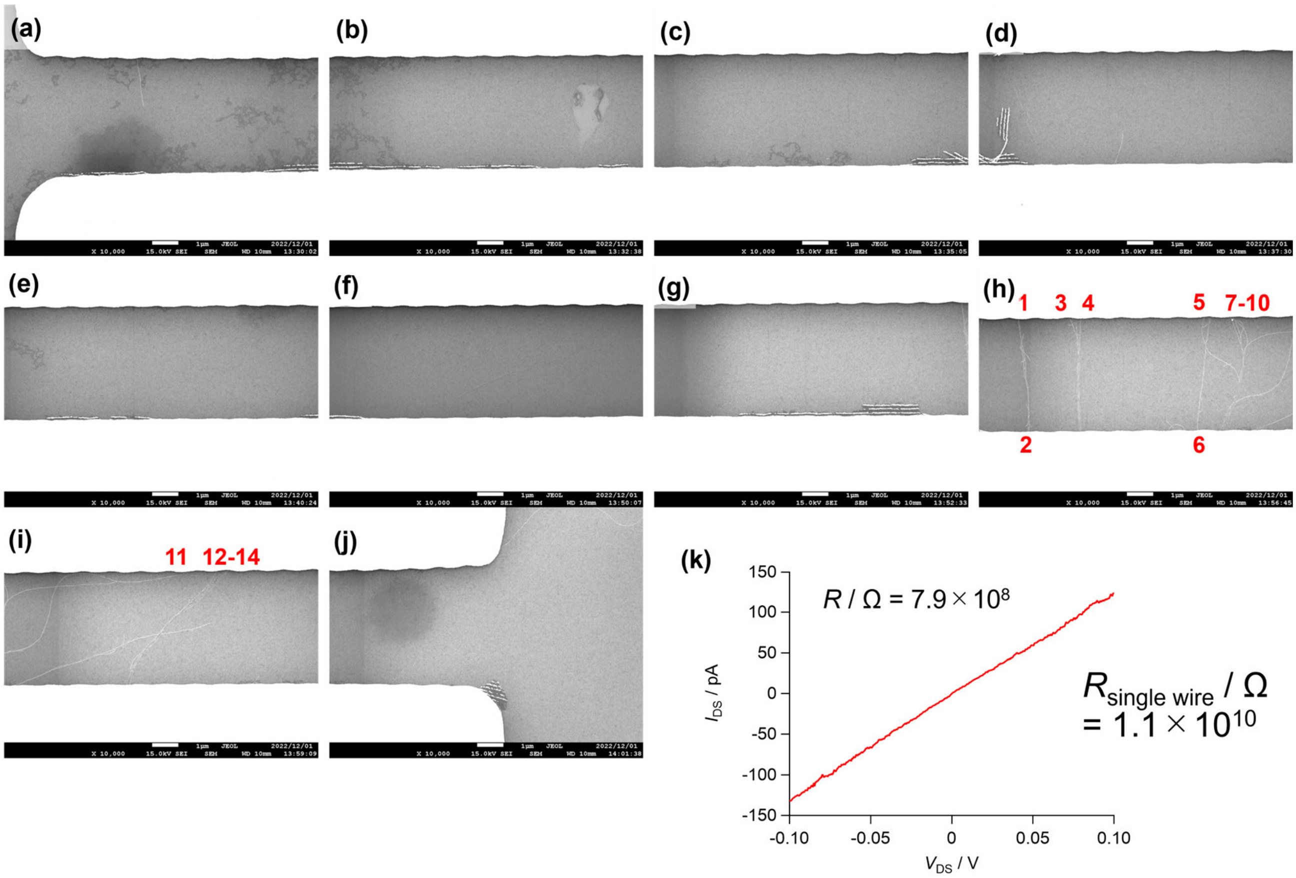

Fig. S7. Electrical characterization at the low fluence. (a-j) SEM images of horizontally-aligned nanowire device at $f = 1\times10^9$ cm^{-2}, $W = 200$ µm. The SEM images were segmented sequentially from (a) to (j) from the original image. In these SEM images, the white areas at the top and bottom are gold electrodes, and the number of cross-linked nanowires is indicated by red numbers. (k) *I-V* curve in this device, which is linear. The electrical resistance of single nanowires was determined using the number of cross-linked nanowires.

2.8. TEM images of C_{60} nanowires

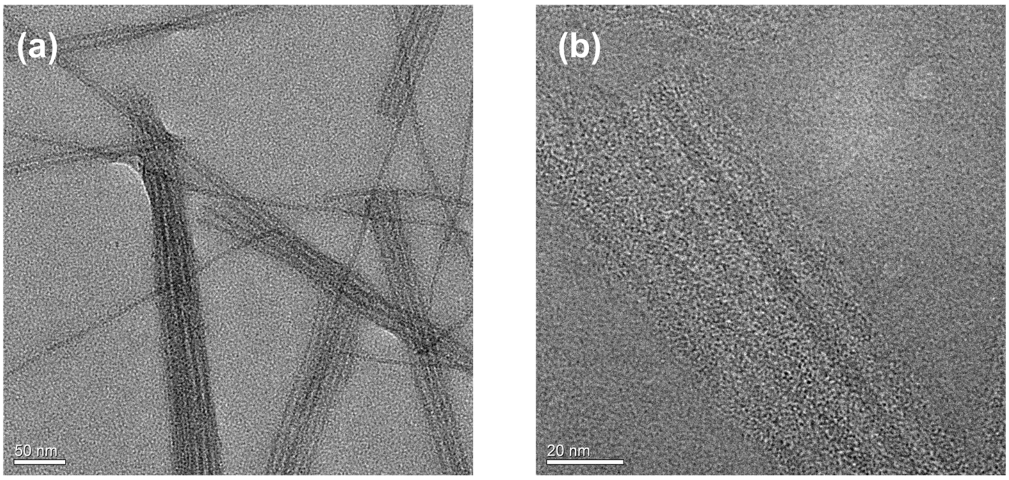

Fig. S8. TEM images of isolated C_{60} nanowires. These nanowires were developed using ODCB, and a dispersion solution was prepared by sonication in ethanol, which was then measured using cryo-TEM.

2.9. Temperature-dependent electrical conduction measurement of C_{60} nanowires

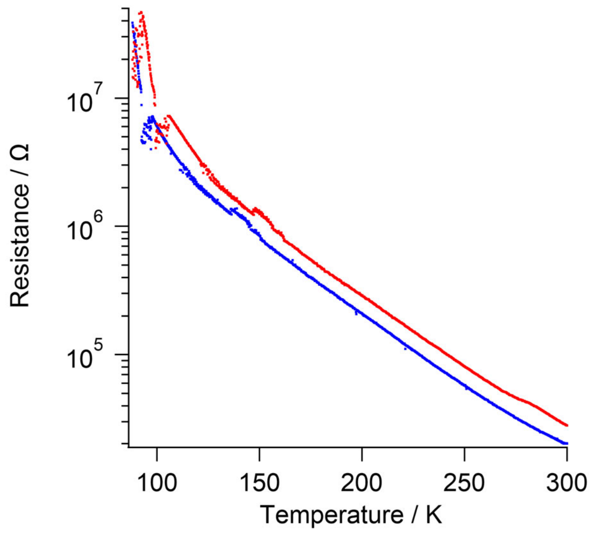

Fig. S9. Temperature dependence of electrical resistance of C_{60} nanowires. The blue marks indicate the cooling process, and the red ones indicate the heating process.

2.10. Conduction model fitting of C_{60} nanowire

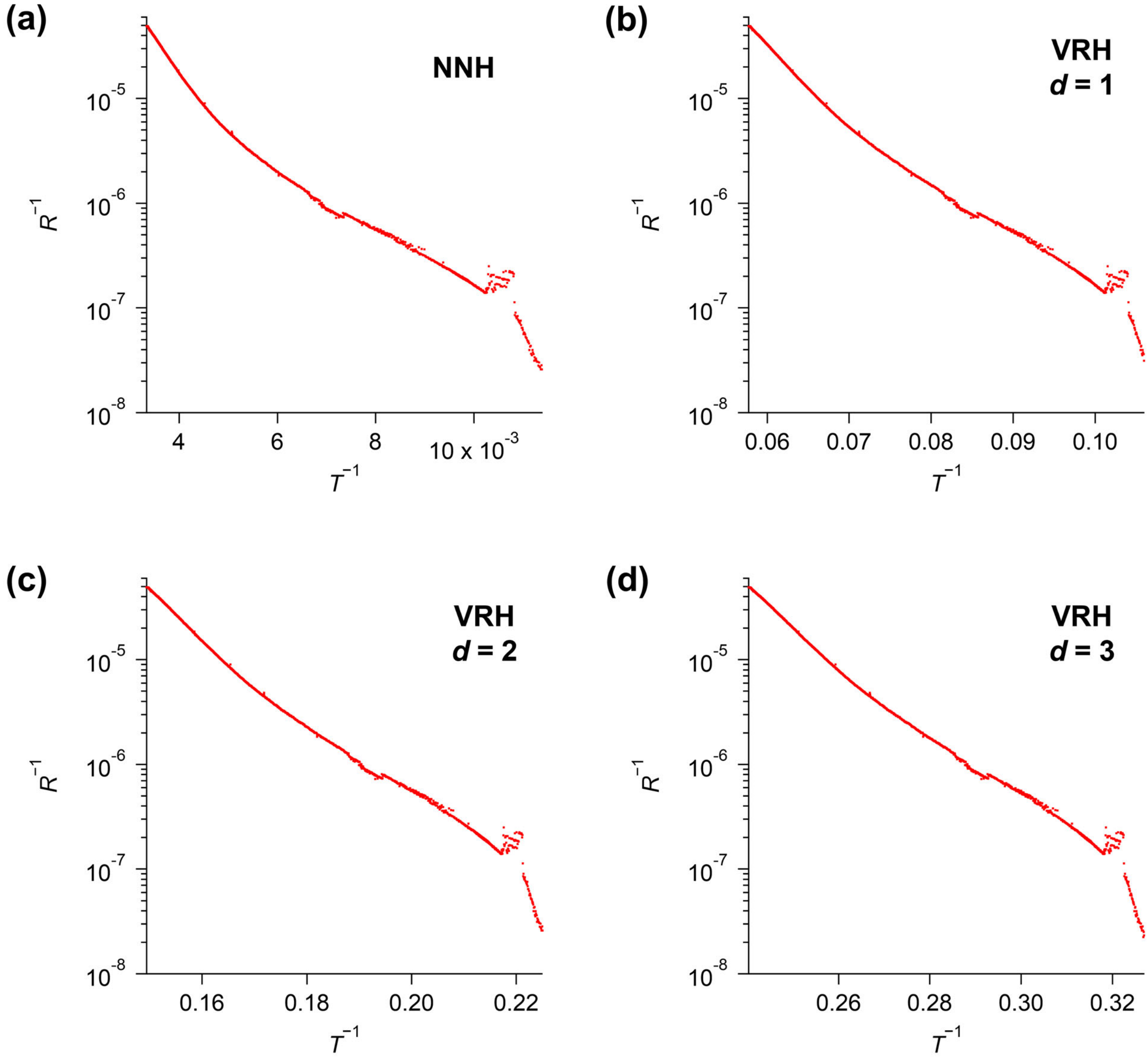

Fig. S10. NNH and VRH model of electrical resistance of C_{60} nanowires. (a) NNH model and (b-d) VRH model of electrical resistance of C_{60} nanowires.

2.11. FET characteristics of C_{60} nanowires

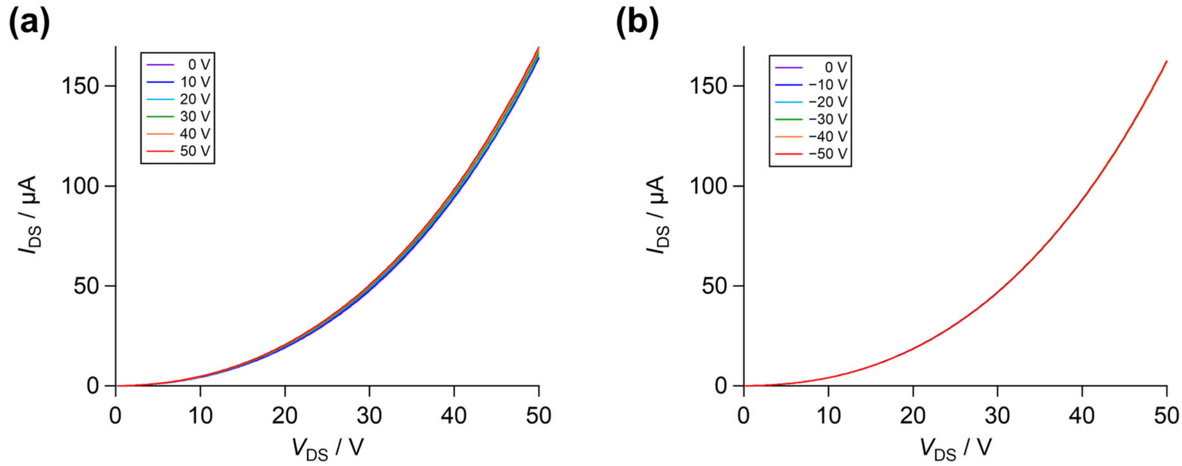

Fig. S11. FET characteristics of C_{60} nanowires. *I-V* characteristics (I_{DS} vs. V_{DS}) at (a) V_G = 0 to 50 V and (b) V_G = 0 to −50 V in a step of 10 V. These measurements were fixed for W = 1500 μm and $f = 1\times10^{11}$ cm^{-2}.

2.12. FET characteristics with respect to gate voltage

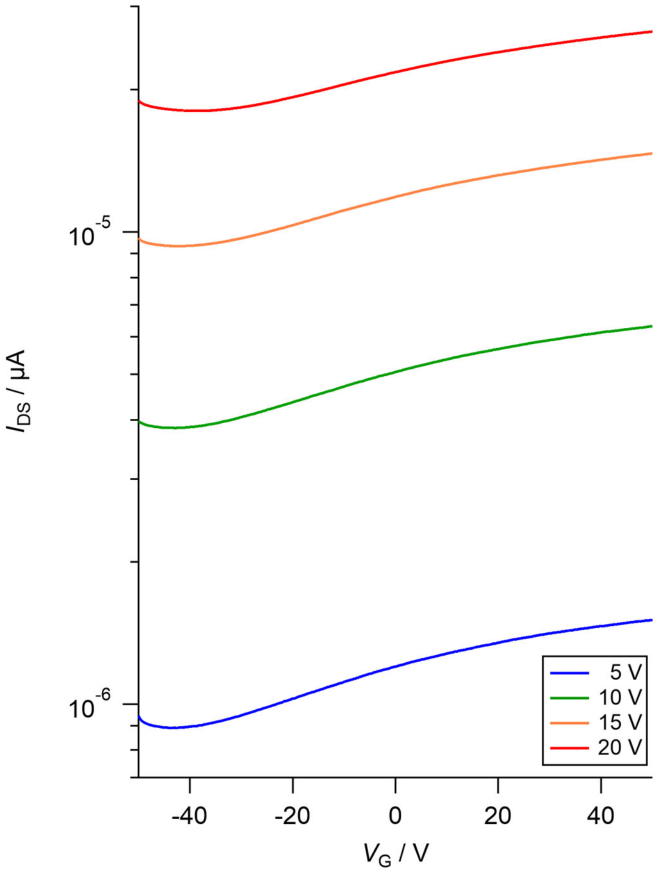

Fig. S12. FET characteristics of C_{60} nanowires. *I-V* characteristics (I_{DS} vs. V_G) at V_{DS} = 5 V (blue), 10 V (green), 15 V (orange), and 20 V (red), respectively. These measurements were fixed for W = 1500 µm and $f = 1\times10^{11}$ cm^{-2}.

2.13. FET characteristics with respect to gate voltage

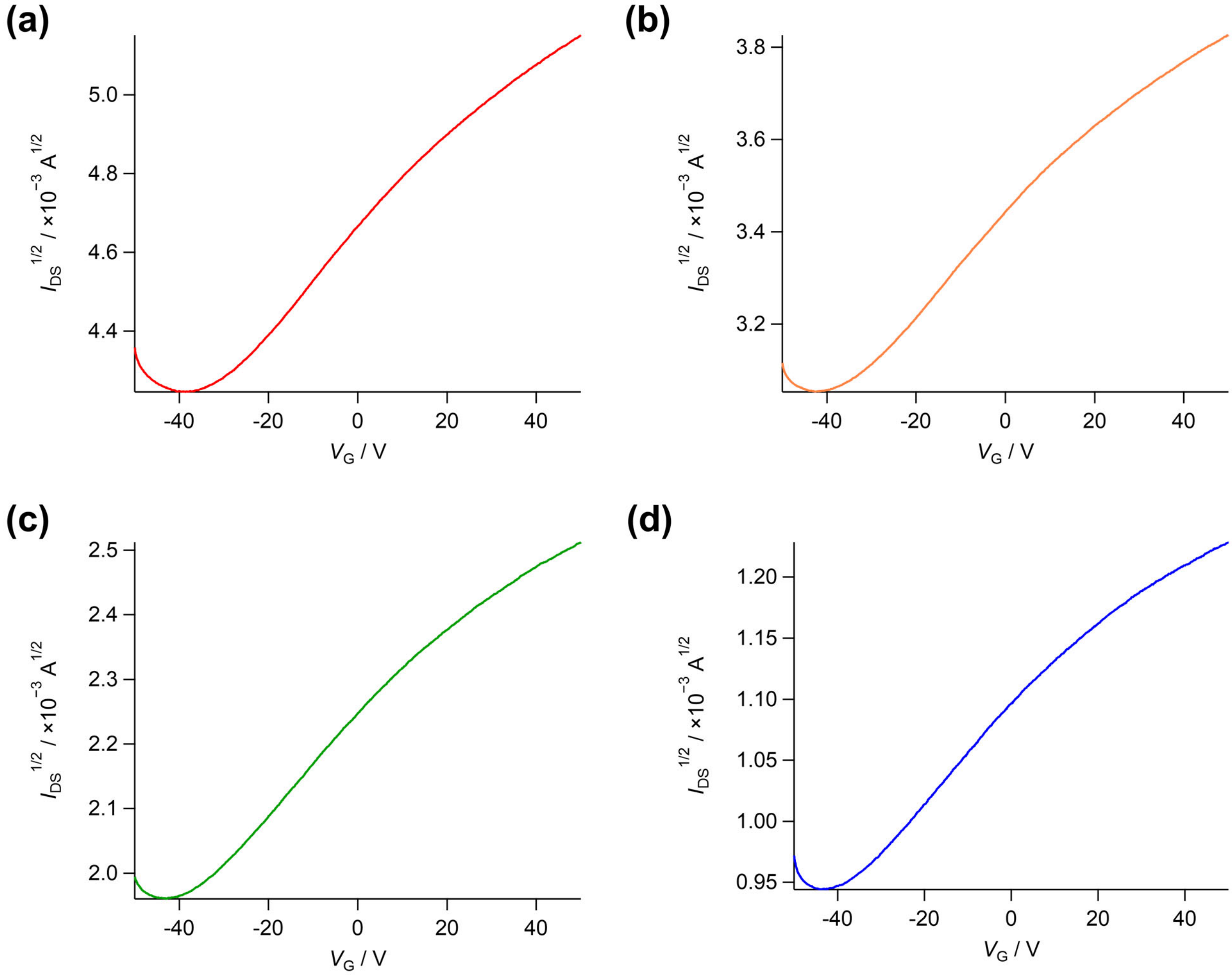

Fig. S13. FET characteristics of C_{60} nanowires. *I-V* characteristics (I_{DS} vs. V_G) at V_{DS} = (a) 20 V, (b) 15 V, (c) 1 V, and (d) 5 V (red), respectively. These measurements were fixed for W = 1500 μm and $f = 1{\times}10^{11}$ cm^{-2}.

2.14. FET characteristics with adsorption of nitrobenzene

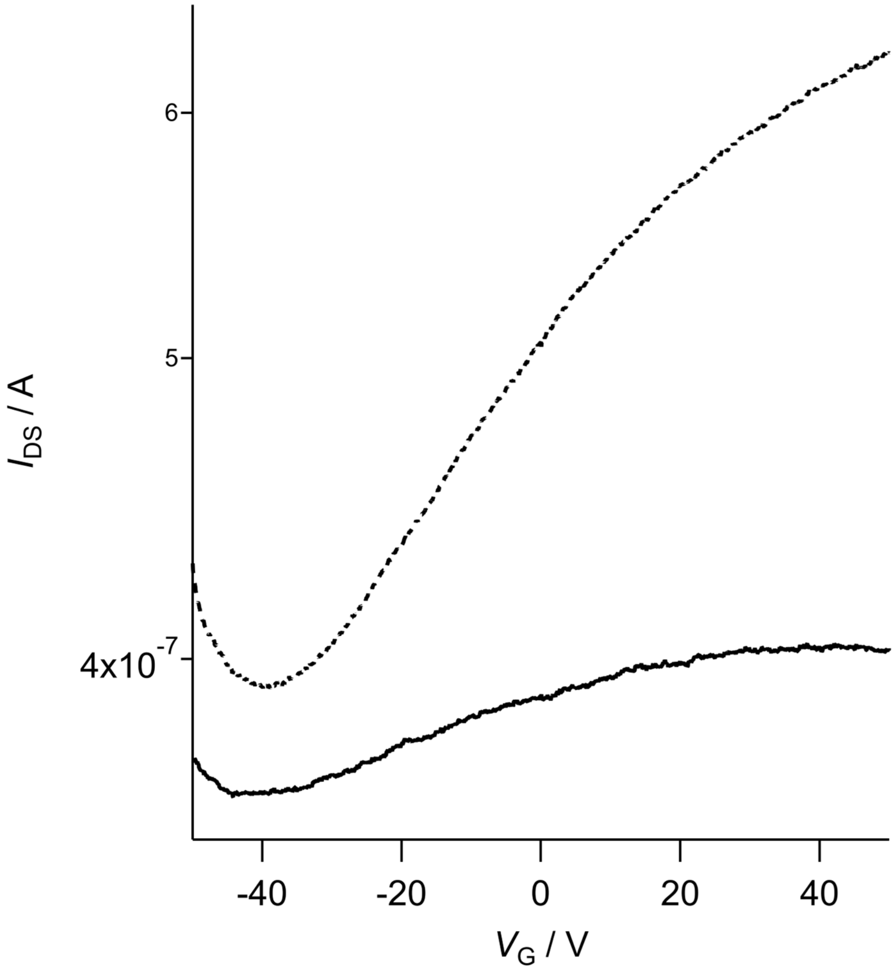

Fig. S14. Electrical conduction property changes due to gas molecule adsorption. *I*-*V* characteristics (I_{DS} vs. V_{DS}), at $V_G = 0$, before (dotted line) and after (solid line) adsorption of nitrobenzene. These measurements were fixed for $W = 1500$ µm and $f = 1\times10^{11}$ cm^{-2}.

2.15. FET characteristics with adsorption of nitrobenzene

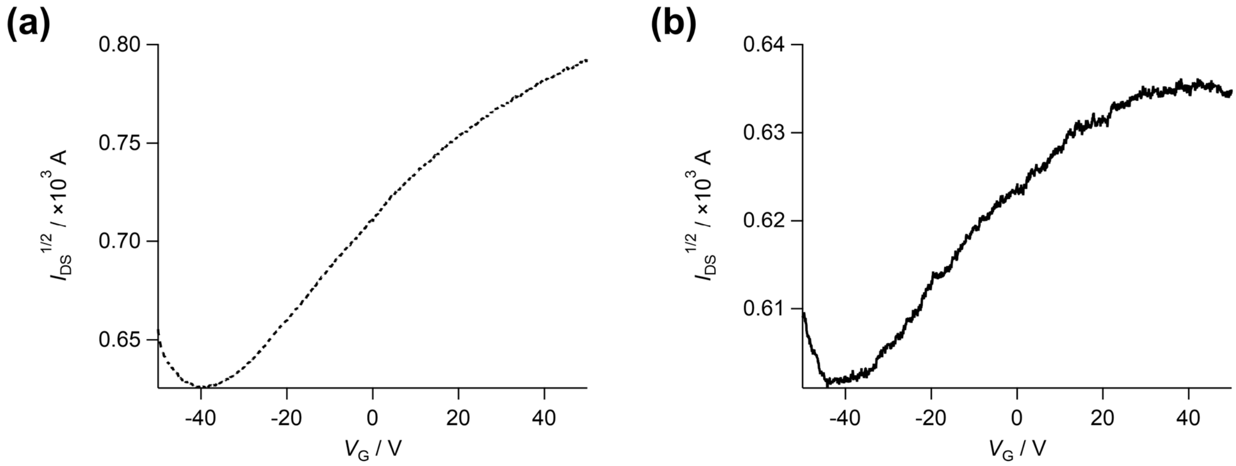

Fig. S15. Electrical conduction property changes due to gas molecule adsorption. *I*-*V* characteristics (I_{DS} vs. V_{DS}), at $V_G = 0$, (a) before and (b) after adsorption of nitrobenzene. These measurements were fixed for $W = 1500$ μm and $f = 1\times10^{11}$ cm^{-2}.

2.16. FET characteristics under vacuum and in the air

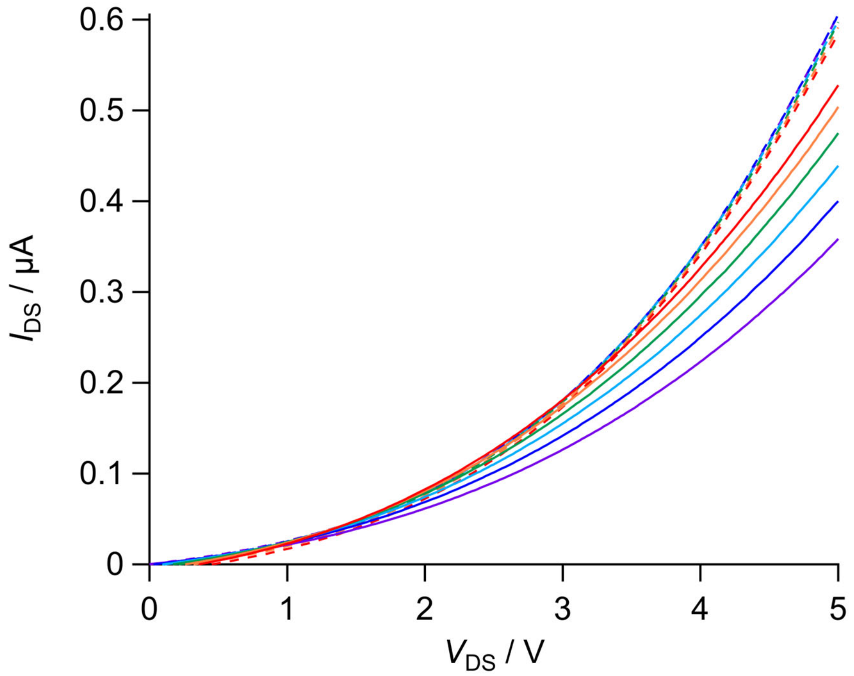

Fig. S16. FET characteristics of C_{60} nanowires in the atmosphere. *I*-*V* characteristics (I_{DS} vs. V_{DS}) at (a) $V_G = 0$ to 50 V and (b) $V_G = 0$ to −50 V in a step of 10 V (dotted line: atmosphere, solid line: vacuum). These measurements were fixed for $W = 1500$ μm and $f = 1\times10^{11}$ cm^{-2}.

2.17. FET characteristics under vacuum and in the air

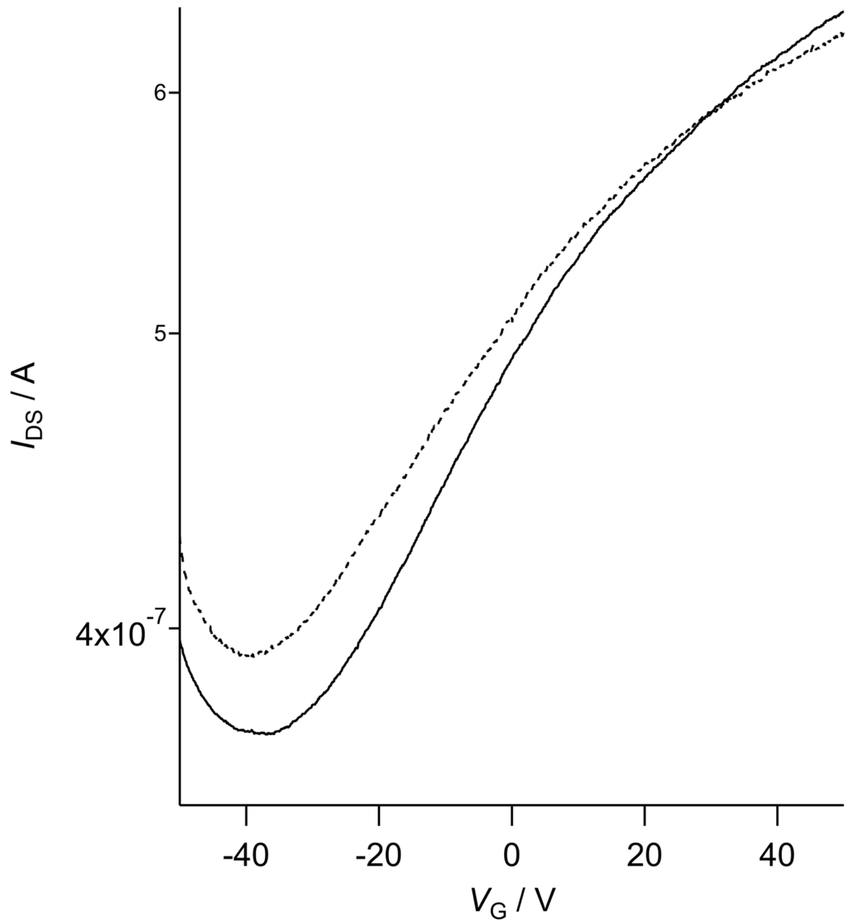

Fig. S17. FET characteristics of C_{60} nanowires in the atmosphere. *I*-*V* characteristics (I_{DS} vs. V_G) at V_{DS} = 5 V. (dotted line: atmosphere, solid line: vacuum). These measurements were fixed for W = 1500 μm and $f = 1\times10^{11}$ cm^{-2}.

2.18. FET characteristics under vacuum and in the air

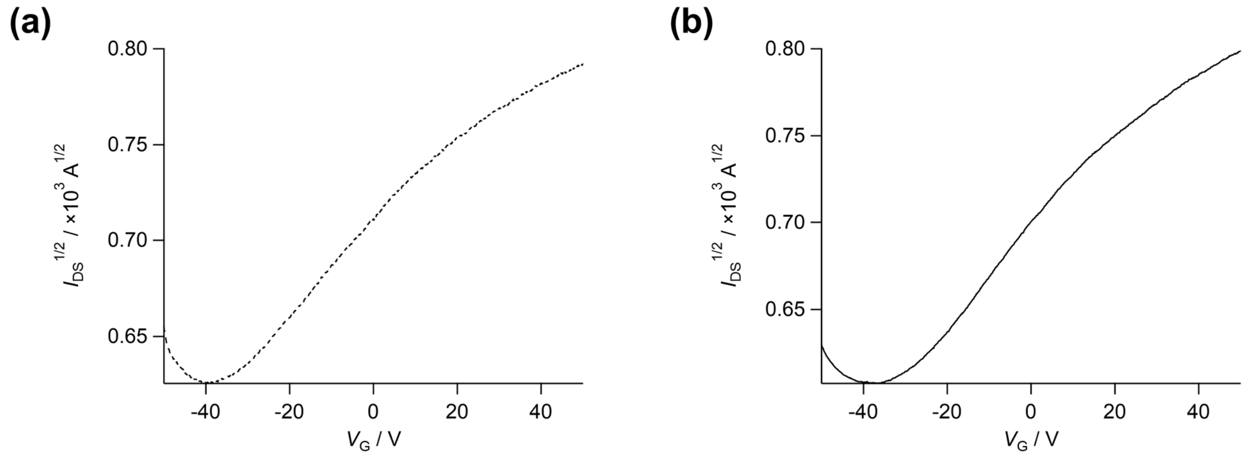

Fig. S18. FET characteristics of C_{60} nanowires in the atmosphere. *I-V* characteristics (I_{DS} vs. V_G) at V_{DS} = 5 V. ((a) atmosphere, (b) vacuum). These measurements were fixed for W = 1500 μm and f = 1×10^{11} cm^{-2}.